Development and calibration of a crossing panel model – Comparison of beam and 3D representations of the crossing rail

Henrik Vilhelmson[1], Björn A. Pålsson[1], Jens C. O. Nielsen[1], Uwe Ossberger[2], Michael Sehner[3] and Harald Loy[3,4]

[1] Department of Mechanics and Maritime Sciences, Chalmers University of Technology, SE–412 96 Gothenburg, Sweden
[2] voestalpine Railway Systems GmbH, 8740 Zeltweg, Austria
[3] Research & Development, Corporate Development, Getzner Werkstoffe, Bürs, Austria
[4] Department of Infrastructure, Unit of Intelligent Transport Systems, University of Innsbruck, Innsbruck, Austria
Henrik.Vilhelmson@chalmers.se

Abstract. This paper presents a finite element model of a railway crossing panel for use in multibody simulations (MBS). It is a two–layer track model with rails and sleepers represented by beam elements, and a crossing rail represented by three-dimensional (3D) solid elements. The track model uses linear bushings for rail fastenings and bi–linear bushings for ballast to allow for potential voids between sleepers and ballast. The model is calibrated and validated to measurement data from a comprehensively instrumented switch & crossing (S&C) demonstrator installed in the Austrian railway network as a part of the European research programme Shift2Rail. A parameterisation with eight parameters relating to track stiffness and ballast voids is introduced to enable the calibration. In a comparison it is shown that the 3D model and a more conventional beam model of the crossing show similar levels of agreement against the measurement data. The 3D model has an increased computational time of about 25% compared to the beam model.

Keywords: railway, switches & crossings, turnout, measurements, 3D finite element model, multibody simulations, dynamic vehicle–track interaction, calibration, response surface

1 Introduction

A fixed crossing allows for trains to cross intersecting tracks. In the wheel transfer from wing rail to crossing nose, the conicity of the wheel in combination with the variation in rail geometry along the crossing results in a wheel–rail excitation that is characterised by a dip in the vertical wheel trajectory. This leads to wheel–rail impact loading and subsequent damage of the running surfaces of wheels and rails (plastic deformation, rolling contact fatigue and wear), noise and vibration and differential settlement of ballast. It can also lead to rail fatigue due to bending and sleeper cracking if the crossing is not maintained properly. Efforts to reduce the consequences of these impact loads is therefore of essence.

As a part of the European Research programme Shift2Rail, a comprehensively instrumented S&C demonstrator has been installed in the Austrian railway network. It has design features such as soft rail pads to reduce impact loading and improve S&C performance.

To evaluate the structural loading in crossing panels due to dynamic vehicle–track interaction, a finite element track model using beam elements was developed in [1]. In [2], the model was calibrated against measured track responses from the Austrian demonstrator. In the calibration, a parameterisation for the void distribution below the crossing transition sleeper and the stiffnesses of rail fastenings and ballast was introduced. The calibration of the model was then based on the minimisation of an objective function comprising a weighted sum of the root mean square error in measured and simulated displacements, strains and sleeper–ballast contact forces. It was found that the agreement between simulation and measurement could be improved by enhanced modelling detail, especially for local strains in the crossing rail that are difficult to estimate with beam theory. In this paper, the track model has therefore been enhanced by modelling the crossing rail using 3D solid elements.

2 Simulation model

The structural finite element model is implemented in the FE-model of the crossing rail and MBS-model can be seen in figure 1. The vehicle model used in this study is a bogie with half of the car body mass on top. The track and vehicle models are described in detail in [2]. The initial condition of the model is determined by finding the static equilibrium for each evaluated track configuration before the start of time-domain simulation.

2.1 Solid element model

The turnout model represents a 60E1-500-1:12 demonstrator installed in the Austrian network as a part of the In2Track projects in the EU-sponsored Shift2Rail research programme.

A 3D finite element model of the crossing is created and meshed using 3D solid second-order elements (primarily tetrahedral elements). To connect the

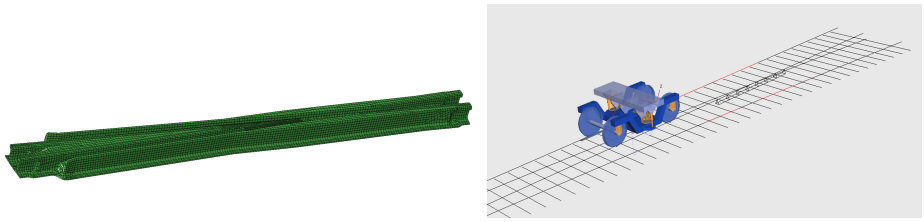

Fig. 1. FE-model of the crossing rail (left). MBS-model (right).

crossing rail modelled with 3D elements to the adjacent rails which are made up of beam elements, the Abaqus [3] keyword **Coupling* in conjunction with the **Distributing* option is used to couple a single beam node to each rail end surface on the crossing. This option couples the displacement and rotation of the beam node to the average displacement of the surface nodes. For each FE-representation of a sleeper or rail body included in the MBS-model, a Craig-Bampton reduction is applied by using the Abaqus **Substructure generate* command. For more detailed information about Craig-Bampton model reduction, see [4].

3 Sensors outputs

The crossing panel instrumentation that is used for the validation and calibration is presented in figure 2. The sensor groups used in the calibration process are presented as groups A to F. Sensors in group A are sleeper–ballast contact pressure sensors placed between between sleeper and under sleeper pad [5], groups B, C and D are all placed on the sleeper, B and C are accelerometers and D strain gauges, while groups E and F are placed on the crossing rail, E is an accelerometer and F consists of strain gauges. The acceleration signals from the instrumented demonstrator are reconstructed to displacements using the method developed in [6].

To compare the response of the simulation model with the measurement data, signals from the simulation model that correspond with the sensors in the measurement setup need to be calculated. Based on the nodal displacements that are directly available as outputs from the simulation, the strains and sleeper–ballast pressure corresponding with measurement sensors can be calculated. The sleeper–ballast pressure and sleeper strains can be calculated using the methods presented in [2], while a new approach for calculations of strains in the crossing rail is presented below.

3.1 Strain

To enable comparison between sensor and simulation results, the strain must be calculated for a position that corresponds to the relevant sensor. This is straightforward if the position corresponds to one of the retained nodes in the

Craig-Bampton reduction. If this is not the case, the displacement of the retained dofs $\boldsymbol{p}^R$ can be transformed into the displacement vector $\boldsymbol{u}$ of the original system using a transformation matrix $\boldsymbol{T}$, see [4]. When the original displacement field has been acquired it can be used to approximate the strain with the engineering strain between two points representing sensor j with the initial length L_j and the displaced length $L_j + u_j$ as

$$\epsilon_j = \frac{L_j + u_j}{L_j} \tag{1}$$

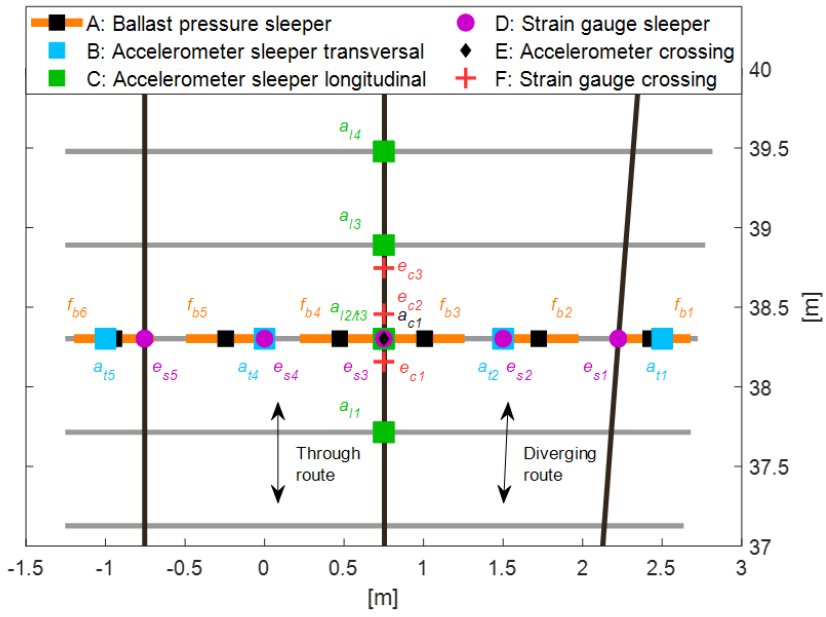

Fig. 2. Sensor groups, locations and labels in the instrumented crossing panel.

4 Model calibration

The model was calibrated for a locomotive run in the through route at 120 km/h. To ensure that the calibration was robust, the calibrated model was evaluated against data from other speeds.

4.1 Model parameterisation

The stiffnesses of ballast and rail fastenings are parameterised in the model. The ballast was parameterised using six local parameters for voids (g_p, $p = 1, 2, ...6$)

under the sleeper at the crossing transition and one uniform ballast stiffness scaling parameter for the entire track model (h_1). The rail fastening stiffness is parameterised by a stiffness scaling parameter (h_2). The distribution of voids along the sleeper is linearly interpolated from the six parameters. An arbitrary void distribution is illustrated in figure 3.

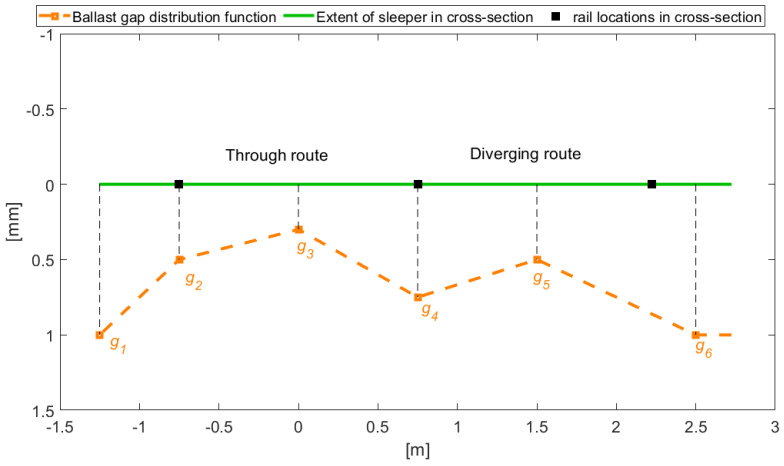

Fig. 3. Illustration of the arbitrary ballast void function.

4.2 Calibration method

The calibration consisting of two steps follow the same method as in [2]. First 500 parameter sets are generated using Latin hypercube sampling (LHS) [7]. From the results of the LHS generated simulation runs a response surface of the objective function is created using a polyharmonic spline. Based on the response surface, a sensitivity study of the model is carried out. From this, the initial parameter intervals are reduced and 500 new sets are generated. In addition, 256 sets are generated covering all boundary combinations of the parameters. This is done to increase the accuracy of the response surface near the boundaries, where the accuracy of radial basis functions is lower [8]. The calibration is then performed by applying a gradient-based optimisation method using *fmincon* in Matlab R2021 [9]. It uses the *interior-point* algorithm to find the best parameter set, i.e the minimum of the response surface.

5 Comparison between beam and 3D models

5.1 Nominal comparison of the models

For the assessment of the beam and 3D models, the sensor outputs from the measurements and the nominal simulation models are plotted. For most channels,

such as the sleeper–ballast contact force or sleeper displacements the extension to 3D did not affect the results significantly, see for example the sleeper displacements in figure 4. However, the implementation of the 3D crossing rail model shows a significant effect on the sleeper strain. This is due to the implementation of the rail pad connected to the crossing rail, which is modelled with one and two bushing elements for the beam and 3D models respectively. This results in different distributions of shear force and bending moment in the sleeper near the lateral position of the crossing rail.

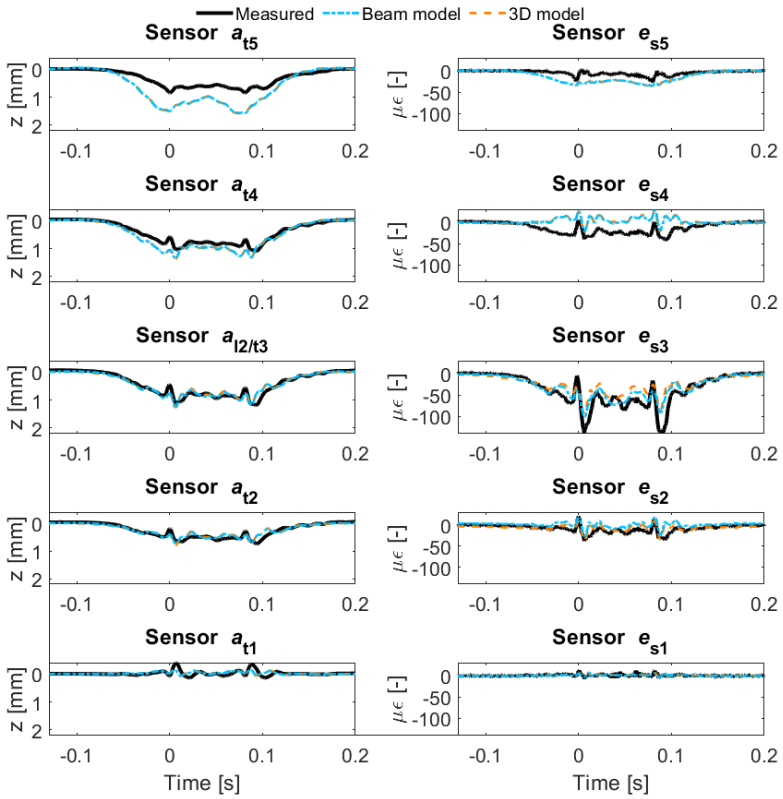

Fig. 4. Displacements ($a_{t1} - a_{t5}$) and strains ($e_{s1} - e_{s5}$) along the sleeper at the crossing transition. See 2 for sensor locations.

5.2 Calibration of the models

The calibration improves the agreement of the model to the measurement data. Before the calibration, the largest discrepancy could be seen in the sleeper–ballast

contact pressure below the crossing sleeper, especially at lateral positions near the crossing rail. The nominal and calibrated sleeper–ballast contact pressures for the six sensors along the sleeper are presented in figure 5, where improvements can be seen for all sensors but most notably for the sensors near the crossing rail.

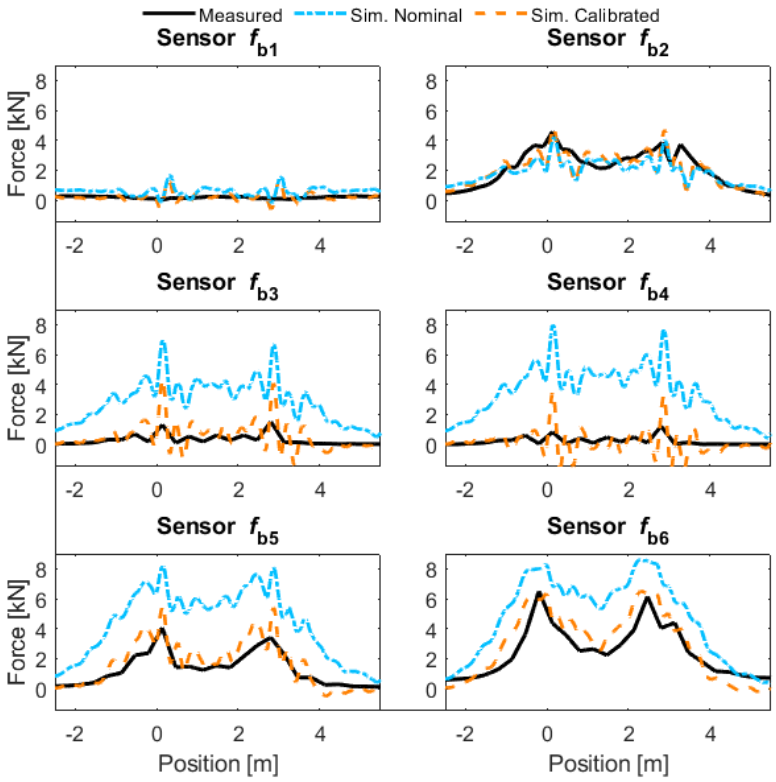

Fig. 5. Sleeper–ballast pressure for the crossing sleeper, see figure 2 for sensor locations.

When comparing the calibrated model from [2] to the calibrated model in this paper, the values for the objective functions of the two models are within 5% of each other.

5.3 Frequency response functions

For a force excitation applied on the crossing nose, the direct receptance has been calculated in figure 6 to compare the receptance of the two models. Very good agreement between the receptance of the two track models is observed below 250 Hz. For higher frequencies, the receptance of the two models diverge.

This indicates that the 3D model is needed to capture high-frequency behaviour more accurately, although it should be noted that the receptance is significantly lower at higher frequencies.

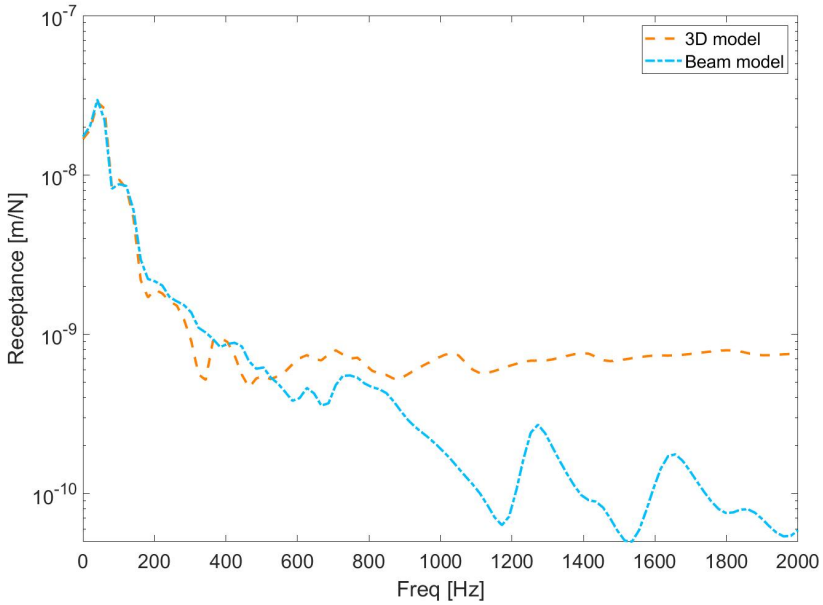

Fig. 6. Frequency response function for the rail displacement at the crossing nose.

5.4 Computational effort

Because the simulation model makes use of substructures, the increase in number of degrees of freedom (dofs) when shifting from beam model to 3D model can be kept quite low. As can be seen in table 1, the increase in dofs is only 106 when using the 3D model. However, the computational time for the static equilibrium and subsequent time integration is increased quite significantly. In addition, time stepping limitations issues for certain parameter settings have been prevalent in the 3D model. Due to the fact that the rail and sleeper body properties are not included in the parametrisation, one set of substructures can be used independent of parameter settings. Therefore substructure generation time has not been included in the CPU time. For a parameterisation where new substructures would have to be generated for each run, the CPU time for the 3D model would increase by an additional 10% compared to the beam model.

Table 1. Comparison of number of degrees of freedom and computational time for the two models.

	Beam	3D
Degrees of freedom	798	904
CPU time [min]	30	40

6 Conclusion

The crossing rail receptance of the beam model is in good agreement with the 3D model up to approximately 250 Hz, which covers the most significant frequency range. However, for improved accuracy at higher frequencies the 3D model is necessary.

Extending the crossing rail model to 3D does not improve agreement with measurement data significantly from the already very accurate beam model. It does however enable detailed calculations of stress and strain fields in the crossing rail and provides more realistic distributions of bending moment and shear force along the sleeper. While the increase in computational time is reasonable, it may be argued that the limited increase in accuracy does not motivate the use of a 3D model for this study where the channels of interest are below 250 Hz.

References

1. Pålsson B.A. A parameterized turnout model for simulation of dynamic vehicle–turnout interaction with an application to crossing geometry assessment. In: Klomp M, et al. (editors). Advances in dynamics of vehicles on roads and tracks. IAVSD 2019. Cham:Springer; 2020. (Lecture Notes in Mechanical Engineering). doi:10.1007/978-3-030-38077-9_41.
2. Pålsson B.A et al. Dynamic vehicle–track interaction and structural loading in a crossing panel – Comprehensive field measurements and calibration of a simulation model. (Submitted for international publication), Department of Mechanics and Maritime Sciences, Chalmers University of Technology, Gothenburg, Sweden 2023.
3. Abaqus. Dassault Systemes; 2018.
4. Craig, R.R, Bampton M.C.C. Coupling of substructures for dynamic analyses. AIAA J. Am. Inst. Aeronaut. Astronautics 6(7), 1313–1319, 1968.
5. Loy H et al. Switches & crossings: Defined elasticity for new turnout designs. Rail Engineering International, 2022.
6. Milosevic M.D.G. Towards model-based condition monitoring of railway switches and crossings. Lic. thesis, Department of Mechanics and Maritime Sciences, Chalmers University of Technology, Gothenburg, Sweden 2021.
7. Olsson A, Sandberg G, Dahlblom O. On Latin hypercube sampling for structural reliability analysis. Struct Saf. 2003;25(1):47-68.
8. Fasshauer GF. Meshfree Approximation Methods with MATLAB. World Scientific Publishing Co Inc, USA; 2007.
9. Matlab R2021. The Mathworks Inc.